# Fiber-Optic Distributed Temperature Sensor Using Incoherent Optical Frequency Domain Reflectometry

Emir Karamehmedović[a] and Ulrich Glombitza[b]

[a] Research Center COM, DTU, Building 345V, 2800 Kgs. Lyngby, Denmark;
[b] LIOS Tech. Gmbh, Schanzenstrasse 6-20, 51063 Cologne, Germany

## ABSTRACT

Distributed temperature sensor based on Raman scattering is investigated. The ratio of intensities in Stokes and anti-Stokes bands reveals the temperature of a fiber section. A spatial resolution of around $1m$ is obtained by use of Incoherent Optical Frequency Domain Reflectometry. An accuracy of $\pm 2K$ is demonstrated over a $16km$ single-mode fiber, which represents a new record. A brief discussion on the choice of the sensing fiber is also given.

**Keywords:** fiber-sensor, frequency domain reflectometry, Raman temperature sensor

## 1. INTRODUCTION

A distributed temperature sensor based on temperature dependent spontaneous Raman scattering in optical fiber is presented. Distributed fiber-sensors are capable of measuring a physical quantity along the fiber length at a number of multiplexed points. If compared with standard electrical sensors, the fiber-optic solution has several significant advantages. Firstly, the vast number of the multiplexed points is accessed by a single line, i.e. the optical fiber itself. Several thousands of electrical point-detectors would demand tremendous cabling. Secondly, the information is carried in the optical domain rather than electrical, rendering the electromagnetic interference harmless for the carried data. A third advantage is total galvanic isolation of the transducer, i.e. the fiber, from the measured medium so that direct contact with the measured object is possible.

Distributed sensors offer the principle of localization known from radar technology. The so-called LIDAR systems can process the received signal in the time or frequency domain, the two techniques being called Optical Time Domain Reflectometry (OTDR) and Optical Frequency Domain Reflectometry (OFDR) respectively. Both techniques have advantages and drawbacks in form of resolution, measurement time, cost and complexity. The resolution here is defined as the spacing between distinguishable adjacent measurement points.

OTDR determines the location of the scattering section by time difference from the emission to the detection of light. This technique requires a high peak-power pulsed laser and fast electronics if high resolution and long range are to be obtained. In OFDR on the other hand, the narrow line-width laser-diode operates in virtually continuous-wave regime. The laser is modulated from DC to RF frequencies and a stationary modulated signal is received in the detector for each modulation frequency. Moreover, using OFDR combined with lock-in techniques, the signal-to-noise ratio (SNR) is improved considerably [1] but the technique introduces some complications as well. Not only the amplitude but also the phases of the signals need to be recorded, setting special demands on electronic components. Furthermore, relatively complex signal processing follows the data-acquisition.

Coherent detection of the optical signal and the reference may ultimately be used to enhance the spatial resolution of the OFDR measuring system down to lengths comparable to the wavelength of the pump laser itself [2] but the range of such a system is limited and does not apply to spontaneous Raman temperature sensing. LIDAR systems based on OTDR Raman scattering with a range of $25km$ and a resolution of $5m$ have been reported [3]. In this paper, the focus is on incoherent OFDR (IOFDR) where a resolution of the order of $1m$ is obtained.

The paper first gives a brief description of the physical principle for measuring temperature using spontaneous Raman scattering. In section 3, the working principle of the IOFDR is described more thoroughly and it is compared with the OTDR technique. Limitations and demands on the system are discussed briefly as well. Section 4 presents the setup and measurement results on 12 km single-mode fiber obtained by IOFRD system. Finally, the main conclusions are drawn in section 5.

## 2. TEMPERATURE DEPENDENT RAMAN SCATTERING

The measuring principle of the described sensor system is based on spontaneous Raman scattering in silica. A solid at a certain absolute temperature $T$ can be regarded as comprised of quantized harmonic oscillators in equilibrium with a gas of phonons [4]. The phonons and the harmonic oscillators of comparable energy can freely exchange energy but the mean number of phonons is constant at a given temperature. Phonons may be described as quasi-particles that obey the Bose-Einstein distribution rendering the probability of phonon creation or annihilation temperature dependent. The mean number of phonons $\bar{n}(\omega_p, T)$ at a given temperature $T$ is thus proportional to the probability for existence of a boson possessing the energy $\hbar\omega_p$.

$$\bar{n}(\omega_p, T) \propto \frac{1}{e^{\frac{\eta\omega_p}{k_B T}} - 1} , \tag{2.1}$$

where $\omega_p$ is the frequency of phonon, $k_B$ the Boltzmann's constant and $\hbar$ Planck's constant ($\hbar = h/2\pi$). In the process of Raman scattering, a pump photon can either absorb or generate a phonon, which adds or subtracts the phonon quantum energy to or from the pump photon energy thus creating an anti-Stokes or Stokes photon respectively.

The intensity of the Stokes line, $I_S$, at a given wavelength $\lambda_S$ is proportional to the intensity of the excitation light, $I_0$, and the probability for creation of a new phonon at frequency $\omega_p$. This probability is proportional to $\bar{n} + 1$ [5]. The intensity of the Stokes line is also inversely proportional to $\lambda_S^4$, just like Rayleigh scattering. Hence,

$$I_S \propto \frac{I_0}{\lambda_S^4} \frac{e^{\frac{\eta\omega_p}{k_B T}}}{e^{\frac{\eta\omega_p}{k_B T}} - 1} , \tag{2.2}$$

Accordingly, the intensity of the anti-Stokes line is proportional to

$$I_{aS} \propto \frac{I_0}{\lambda_{aS}^4} \frac{1}{e^{\frac{\eta\omega_p}{k_B T}} - 1} , \tag{2.3}$$

where the probability for phonon annihilation is assumed to be proportional to $\bar{n}$ [5]. Assuming the created and absorbed phonons posses same energy, i.e., have the same frequency, the ratio between the intensities of the two lines is

$$\frac{I_{aS}}{I_S} = \left(\frac{\lambda_S}{\lambda_{aS}}\right)^4 \cdot e^{-\frac{\eta\omega_p}{k_B T}} . \tag{2.4}$$

From Equation (2.4) it is possible to isolate and determine the absolute temperature unambiguously when both $I_S$ and $I_{aS}$ are known. Point sensors based on the temperature dependent spontaneous Raman scattering are used in e.g. development of gas-turbines or turbine engines [6]. In such measurements, however, the temperature information is provided only for a single point at a time. In the next section, it is shown how to obtain the temperature profile in space, in our case along an optical fiber, using the IOFDR technique mentioned.

## 3. INCOHERENT OPTICAL FREQUENCY DOMAIN REFLECTOMETRY

In this section, a more elaborate introduction to the IOFDR technique is presented. Range and spatial resolution are defined and several factors that limit these values are mentioned. Considerations with respect to the type of the sensing fiber and probe wavelength are made as well.

The intensity of the sinusoidally modulated pump signal that is propagating in the fiber may be expressed as

$$I_P(z, t, \omega_m) = I_0 \cdot e^{-\alpha_P z}(1 + m \cdot \Re e\{e^{i\omega_m(t - \beta_P z)}\}) , \tag{3.1}$$

where $z$ is the distance, $m$ is the modulation depth, $\omega_m$ the radial modulation frequency, $c$ is velocity of light in free space, $n_p$ the refractive index at the pump wavelength $\lambda_P$, and hence $\beta_P = n_P/c$ is the reciprocal of velocity of the light in the fiber. $\alpha_P$ is the attenuation coefficient in the fiber at $\lambda_P$, which is initially assumed to be temperature independent. $I_P$ is a real, positive harmonic function. By use of notation in (3.1), the following derivations are simplified. Ideally the modulation depth would be $m=1$ but it is less than that in order to drive the laser in the linear regime.

The Raman-scattered signals may be written as

$$I_S(z,t) = I_p(z,t)\chi_S(T(z,t)),\qquad(3.2)$$

$$I_{aS}(z,t) = I_p(z,t)\chi_{aS}(T(z,t)),\qquad(3.3)$$

where $T$ is the time- and place dependent absolute temperature, $\chi_R(T(z,t))$ is the temperature dependent scattering coefficient of either the Stokes or anti-Stokes line. Temperature fluctuations are assumed to be much slower than a single measurement so that $T$ is in the following only space dependent. One can say that $\chi_R$ is fiber-specific and thus avoid additional constants that represent different doping levels, different numerical apertures (NA) etc. Because of the obvious similarity in the form of Stokes and anti-Stokes signals, i.e. they differ only in the subscript, capital $R$ is used in the following unless there is a need to distinguish between the two signals.

The backscattered signals originating from a point $z$ and measured at the detectors contain both phase and amplitude information

$$I_R(z,t,\omega_m) = I_0 \cdot \chi_R(T(z)) \cdot e^{-(\alpha_P+\alpha_R)z}(1 + m \cdot e^{i\omega_m(t-(\beta_P+\beta_R)z)}),\qquad(3.4)$$

The received Stokes signal on the detector itself from the entire fiber of length $L$ is a summation from all the infinitesimal fiber sections i.e. the integral

$$I_{R,d}(t,\omega_m) = I_0\left(\int_0^L \chi_R(T(z)) \cdot e^{-(\alpha_P+\alpha_R)z}dz + m \cdot e^{i\omega_m t} \cdot \int_0^L \chi_R(T(z)) \cdot e^{-(\alpha_P+\alpha_R)z - i\omega_m(\beta_P+\beta_R)z}dz\right),\qquad(3.5)$$

For the time being, in (3.4) and (3.5) we choose to neglect the loss originating from splices, optical components and other perturbations of the signals that are specific for a certain setup. The first term in the parenthesis of Equation (3.5) is invariant with respect to the modulation frequency and contains no information on the location from where the Raman scattering originates. We therefore focus on the second, modulation-frequency dependent term

$$\widetilde{I}_{R,d}(t,\omega_m) = m \cdot I_0 \cdot e^{i\omega_m t} \cdot \int_0^L s_R(z) \cdot e^{-i\Omega_{PR}z}dz,\qquad(3.6)$$

where $\Omega_{PR} = \omega_m(\beta_P+\beta_R)$, and $s_R(z) = \chi_R(T(z))\exp(-(\alpha_P+\alpha_R)z)$ contains both the scattering coefficient and the attenuation factor. One can regard the integral of Equation (3.6) as a Fourier transform $S_R(\omega_m)$ of $s_R(z)$. In other words, if inverse Fourier transformation is performed on the array of measured data for each modulation frequency, one can obtain the scattering coefficient as function of distance $z$. Using Equation (2.4) it is possible to derive the temperature distribution along the optical fiber

$$T(z) = T_0 + \frac{\eta\omega_p}{k_B}\left(\ln\left(\frac{R(T(z))}{R_0}\frac{\lambda_{aS}^4}{\lambda_S^4}e^{-\int_0^z(\alpha_{aS}(z)-\alpha_S(z))dz}\right)\right)^{-1},\qquad(3.7)$$

$R(T(z))$ is the ratio between the scattering functions $\chi_{aS}(T(z))$ and $\chi_S(T(z))$ and $T_0$ and $R_0$ are calibration constants. As the attenuation changes with the temperature, for greater accuracy it is necessary to sum the attenuation that is experienced by the wave at each point in the fiber [7].

In OTDR, the spatial resolution is determined mainly by the sampling-rate of the signals, assuming that the pulse width of the pump is shorter than or equal to the sampling period $1/f_{samp}$, and it is only the attenuation in the fiber and hence the sensitivity of the detectors that limit the range of the sensor. If $n_g$ is the group index at pump and Raman-

scattered wavelengths in the fiber, the smallest distance between two measurement points, $\Delta z_{OTDR}$, that is the resolution, is [8]

$$\Delta z_{OTDR} = \frac{c}{2n_g} \frac{1}{f_{samp.}},$$ (3.8)

Equivalently, the spatial resolution of an IOFDR system, $\Delta z_{IOFDR}$, is defined by the maximal modulation frequency of the source $\omega_{m,max} = 2\pi f_{m,max}$, [8]

$$\Delta z_{IOFDR} = \frac{c}{2n_g} \frac{2\pi}{\omega_{m,max} - \omega_{m,min}} = \frac{c}{4n_g} \frac{1}{f_{m,max}} ,$$ (3.9)

In a practical system using FFT algorithms, one cannot resolve more spatial points than the number of measurements/samples in the frequency domain. Therefore, there is an additional restriction for the maximum range $L_{max}$ in the IOFDR system, namely

$$N = \frac{\omega_{m,max}}{\Delta\omega_m} = \frac{L_{max}}{\Delta z_{IOFDR}} ,$$ (3.10)

where $N$ is the number of samples and $\Delta\omega_m$ is the step in modulation frequency. From these equations it follows that the maximum length of the fiber sensor is limited by the step in modulation frequency (assuming sufficient input power to the detector)

$$L_{max} = \frac{c}{4n_g} \frac{2\pi}{\Delta\omega_m} ,$$ (3.11)

## 3.1. Power level limit

Assuming the temperature is constant along the fiber, the Raman scattering coefficient $\chi_R$ becomes constant. The integral of Equation (3.6) is evaluated

$$\tilde{I}_R(\omega_m) = I_0 \cdot \frac{\chi_R}{-\alpha_{PR} + \iota\omega_m\beta_{PR}} \left(e^{(-\alpha_{PR} + \iota\omega_m\beta_{PR})L} - 1\right),$$ (3.12)

where $\alpha_{PR} = \alpha_P + \alpha_R$. It is evident that the magnitude of the signal falls off as the modulation frequency increases. And for a fixed spatial resolution, the maximal modulation frequency is independent on the fiber length. Therefore, using IOFDR, it is not necessarily easier to measure a quantity on shorter fiber-lengths, as is the case for OTDR. From Equation (3.12) one can see that longer fibers in total scatter more radiation than shorter fibers. Consequently, the lowest signal power-level is not a monotonous function of fiber length. In Figure 1(a), the behavior of the normalized and absolute magnitude of $\tilde{I}_R$ is shown for $L = 1km$, $\beta_{PR} = 10^{-8} s/m$ and $\alpha_{PR} = 0.4 dB/km$ (values for standard single-mode fiber) as function of modulation frequency.

Figure 1(b) shows the product of the minimum magnitude of Equation (3.12) for all necessary frequencies and the signal intensity at DC as function of fiber length, corresponding to the relative detector sensitivity required for performing a measurement with 0.5m resolution, that is, with maximum modulation frequency of 100MHz. In other words, the figure shows how much does the signal drop in power from DC value as function of fiber length. The signal intensity of the anti-Stokes channel at DC, when determined experimentally for a certain fiber length, can be used to calculate the least intensity for all fiber-lengths inserting it in Equation (3.6). Typically, the intensity at DC is in the range of several tens to hundreds nanowatt, depending on the fiber length and type. This gives the smallest signal intensity of only a fraction of a pico-watt.

It is found that the lowest signal one needs to detect actually increases by almost an order of magnitude as the fiber length is prolonged from $1km$ to $12km$. The only requirement is that the frequency step $\Delta\omega_m$ needs to be twelve times smaller as shown in Equation (3.11).
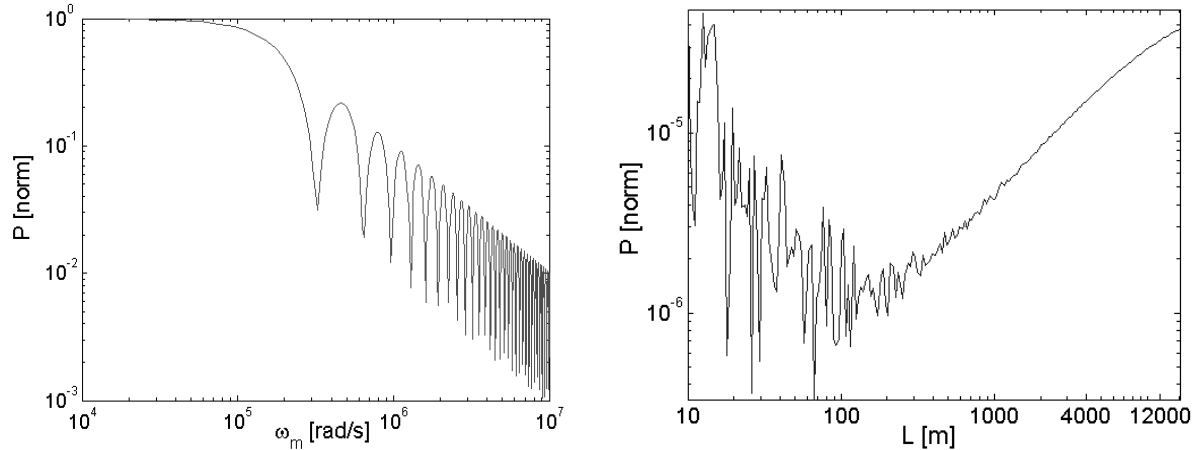
**Figure 1** **(a)** Normalized magnitude of the backscattered signal at the detector as function of modulation frequency. The fiber length is 1*km*. **(b)** The graph shows the product of the least normalized magnitude and magnitude at DC (no modulation) as function of the fiber length.

## 3.2. Choice of the sensing fiber and operating wavelength

There are a number of factors one has to take into consideration when choosing a proper sensor fiber. Clearly, the attenuation has to be low at the operating wavelengths (anti-Stokes, pump and Stokes) to have a detectable signal for relevant fiber lengths. A high capture ratio of the back-scattered light i.e. a large numerical aperture of the fiber is desirable as well. The doping of the fiber is also an issue since e.g. $GeO_2$ doped fiber has a higher Raman scattering coefficient but at the same time higher loss. Finally, the cost of the fiber should not be neglected. The availability of relevant optical components such as filters and multiplexers at the desired wavelengths also play a role in the decision.

The difference in group indices i.e. propagation velocity in the fiber at the pump, Stokes and anti-Stokes wavelengths can also limit the resolution or range of the sensor, as the fiber length is effectively different for the two signals. When this difference in fiber lengths $\Delta L$ becomes comparable to the spatial resolution $\Delta z$, the measurements are no longer accurate as specified.

$$\Delta z_{IOFDR} > \Delta L = N(\Delta z_S - \Delta z_{aS}) = \frac{2\pi Nc}{\omega_{max}} \left| \frac{1}{n_P + n_S} - \frac{1}{n_P + n_{aS}} \right|, \quad (3.13)$$

Assuming the common denominator of the difference in the equation is $4n_g^2$ gives

$$\Delta z_{IOFDR} > N \cdot \Delta z_{IOFDR} \left| \frac{\Delta n}{2n_g} \right| \Leftrightarrow N < \left| \frac{2n_g}{\Delta n} \right|, \quad (3.14)$$

where $N$ is the number of data-points and $\Delta n$ the difference in refractive indices at Stokes and anti-Stokes wavelengths. If the resolution is set to $\Delta z=1m$, $N$ corresponds to the length of the fiber in meters. As an example, a $\Delta n$ of $5 \cdot 10^{-4}$, which is a typical value in multimode fibers (MMF) at around 940*nm* or around 1500*nm* in single-mode fiber, limits the length $L$ to approximately 6*km*. If MMF is used, there is an additional uncertainty due to different propagation velocities of different modes, in which case $\Delta n$ describes the maximum difference in the effective modal dispersion. In case of single mode fiber, it is possible to correct for this error entirely if the effective $\Delta n$ is known.

The finite BL product (transmission Bandwidth × Length) of the sensing fiber may also be limiting factor for high resolution and range measurements, especially in step index MM fibers [1]. Graded-index MM fiber is appropriate choice for sensors of no more than 7*km* in length and spatial resolution of approximately 1*m* – otherwise the signal power is more favorable if SMF is used [1]. Ideally, photonic crystal fiber technology offers special designs with large-mode-area single-mode fiber with high NA, but such fiber is too expensive for this application.

The Raman scattering cross-section peaks at a frequency shift of around $\Delta f=13THz$ for both silica and the usual dopant $GeO_2$. The preferred detectors are Si or InGaAs APDs. The generated signals have to be in the low-loss

interval of wavelengths in the fiber and detectable by the APDs. Systems based on Si APDs and thus MMF would use high power 940-980*nm* single-mode laser. The anti-Stokes and Stokes lie at around 940nm and 1020nm. If SMF is used, it is beneficial to increase the wavelength as much as the detectors and the infrared absorption allow because one should avoid having the anti-Stokes at the absorption peak of the fiber, which is at 1385*nm*. A limit of the Stokes of no more than 1630nm is set if relatively large changes of the APD's responsivity as consequence of temperature fluctuations of the APD itself are to be avoided. Thus, the pump wavelength should be in vicinity of 1500*nm*. The peaks of Stokes and anti-Stokes signals are shifted by around Δλ=100*nm*.

## 4. EXPERIMENTAL SETUP AND MEASUREMENTS

In this work, it is intended to make a 16*km* distributed fiber temperature sensor. Therefore, SMF is chosen and an appropriate 320*mW* pump laser with center wavelength at 1493*nm* is found. Experiments are performed using spools of 4*km* and 12*km* fibers. The entire setup is described in the following section. Hereafter measurement results are presented.

### 4.1. Experimental setup

Figure 2 shows the configuration of the optical system of the sensor. A grating-stabilized single mode laser-diode with maximum output power of 320mW is used as the pump. A fraction of the pump power is detected as a reference before entering the fiber to be able to determine the actual phase shift of the detected Raman scattered signals. The sensing fiber is composed of 4*km* standard SMF and 12*km* long dehydrated SMF.
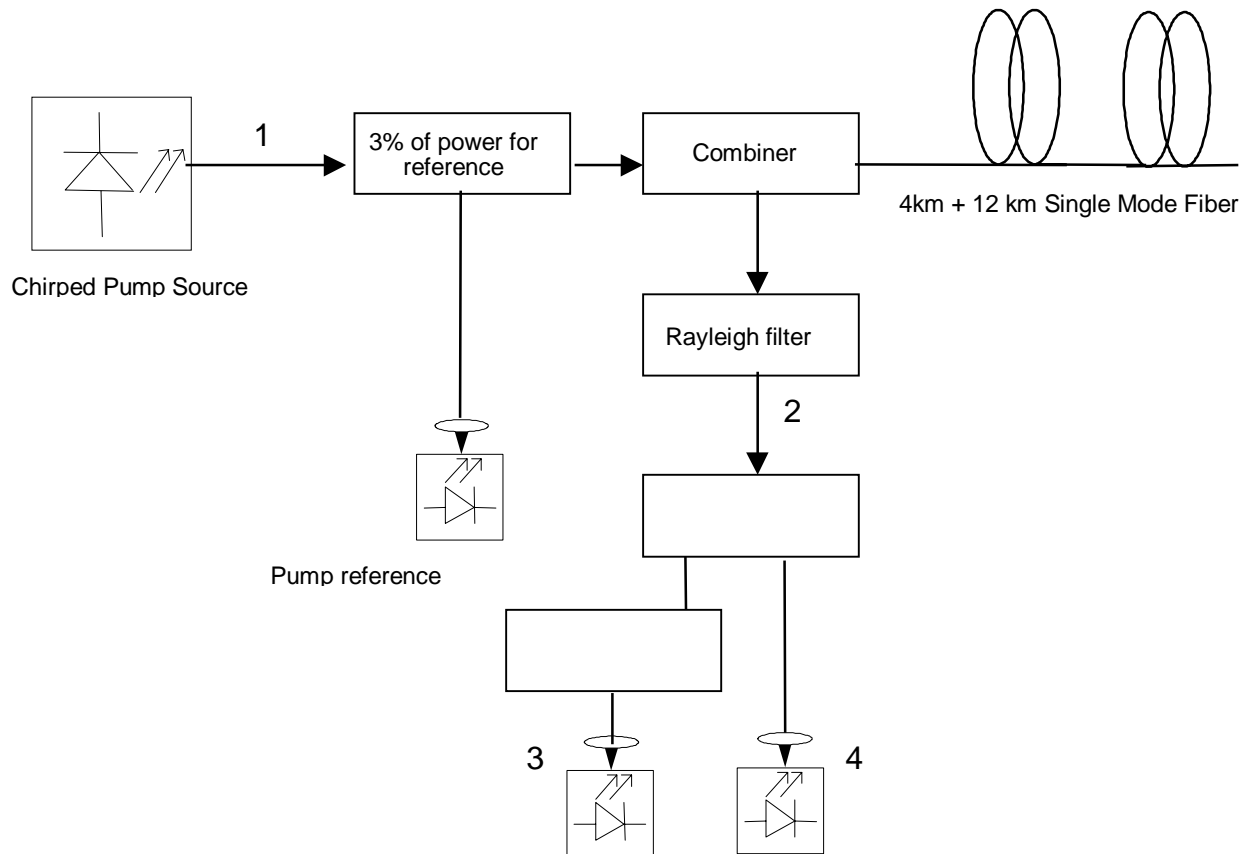


**Figure 2.** Scheme of the optical setup of the measurement system. Optical spectrum at points 1, 2, 3 and 4 are displayed in the following.

Figure 3(a) shows the optical spectrum of the LD, measured at point 1 in the setup. The RMS spectral width of the laser diode is around 1*nm*, which is sufficiently large to suppress Brillouin scattering and thus avoid the associated loss of pump power.

Figure 3(b) shows the backscattered Raman signal where the Rayleigh scattering of the pump is filtered out, i.e., the signal spectrum at point 2 in the setup. One can recognize the shape of the Raman gain function in silica on both sides of the pump. The anti-Stokes signal has been filtered by a 17$nm$ wide bandpass filter centered around 1410$nm$, whereas the Stokes signal has been filtered by a spectrum separator with the center wavelength 1545$nm$.
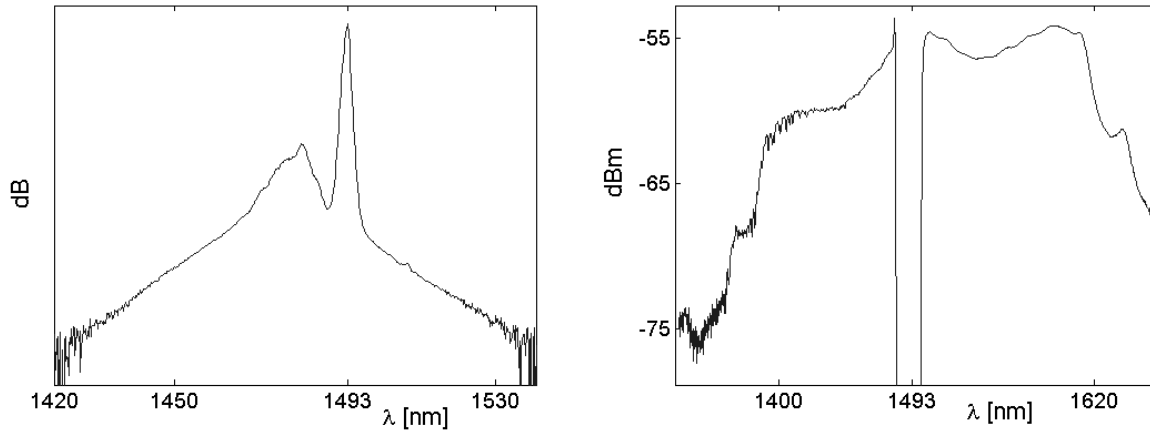


**Figure 3** Signal spectra at points 1 and 2 in the setup respectively. Figure (a) is the spectrum of the pump source. Heating the semiconductor chip reduces the local peak at 1480nm. Anti-Stokes and Stokes signals where Rayleigh scattering is filtered out is shown in Figure (b).

The bands of the anti-Stokes and Stokes are separated and detected by highly sensitive APDs. The signals corresponding to the points 3 and 4 in the setup are shown in Figure 4. When the laser is driven at the maximum output power of 320mW, the power of the anti-Stokes channel is around 40$nW$ at DC (no modulation). According to Figure 1(b), the intensity of the alternating signal at 100$MHz$ modulation would be in $pW$ range.
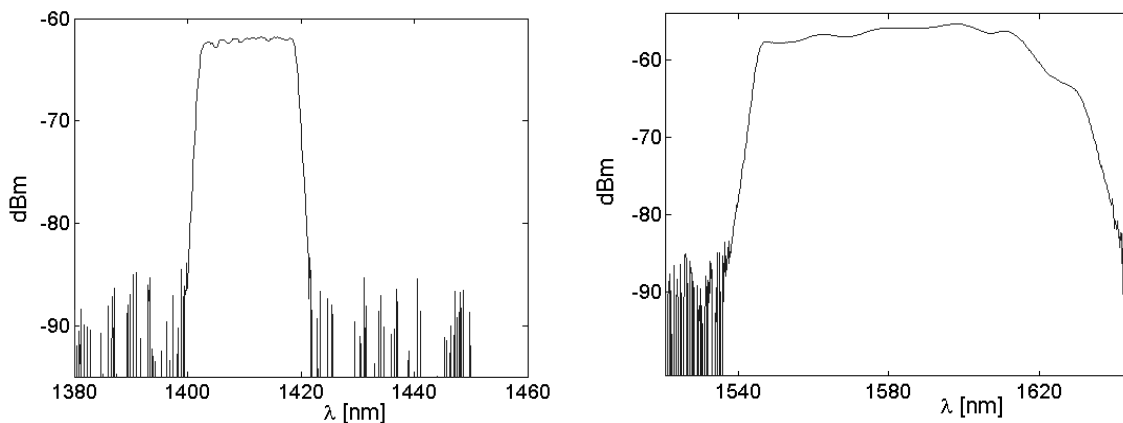


**Figure 4** Filtered anti-Stokes and Stokes signals that appear at the detectors when no modulation is applied to the laser. The signal with least intensity determines the limit of modulation frequency or fiber length, i.e. the range of the sensor. In this case, it is the anti-Stokes signal.

## 4.2 Temperature measurements

The calculation of the inverse Fourier transformation for the complex frequency-measuring data provide the backscattering curves. The processor that is used for signal processing is capable of handling up to 8196 measurements. This limits the resolution of 16$km$ fiber sensor to approximately 2$m$. The maximum modulation frequency of the laser pump is then around 25$MHz$.
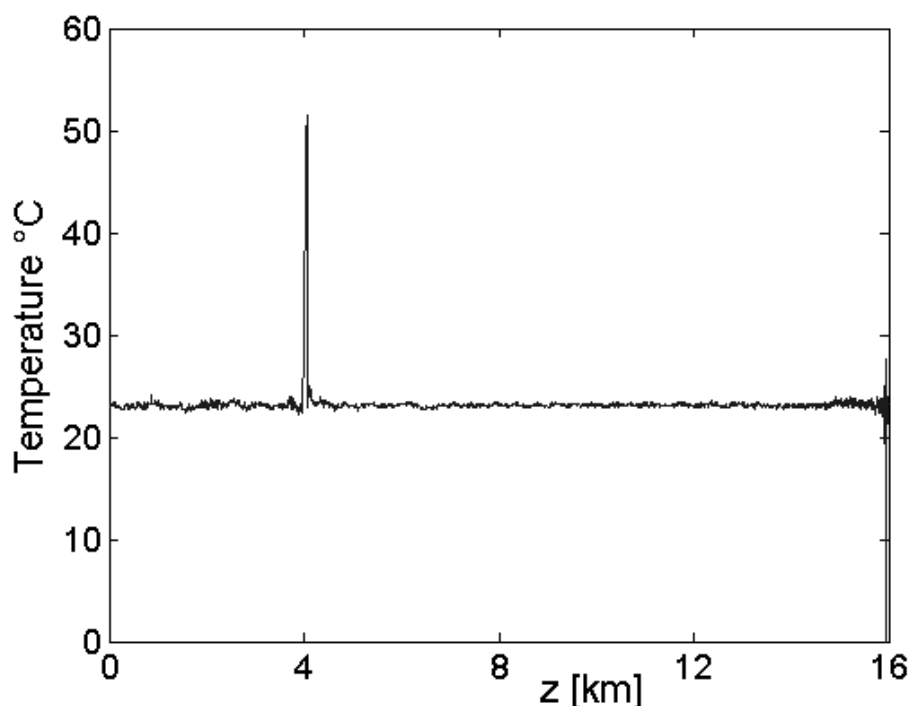
**Figure 5** Temperature profile along 16km of optical fiber. The hot-spot at 4km is evident.

The two fibers that are used in the experiment have different attenuation constants at the anti-Stokes wavelength. Furthermore, the nonlinear response of the pump laser to modulation also affects the data and has to be measured. Additional signal processing is done to rectify the temperature-distance curve. After numerical corrections, the temperature at spatially distributed points along the fiber is shown in Figure 5.

A section of 40$m$ of the fiber in between the two spools is submerged in hot water. The temperature of the water is measured by a thermistor and it is stabilized at 51°C. A clear peak in temperature is seen at the junction between the two coils. The rest of the fiber is at room temperature, in this case it is 23°C.

Due to the increasing total attenuation that the waves experience as they propagate further into the fiber, the uncertainty in measurements grows accordingly.

## 5. CONCLUSIONS

A distributed temperature sensor based on spontaneous Raman scattering in single-mode fiber has been demonstrated. A brief theoretical description of the IOFDR technique for spatial resolution of the backscattered waves has been given.

Measurements on 16$km$ of SM fiber with spatial resolution of 2.1$m$ have been presented. To the best of the authors' knowledge, this represents a new record for an IOFDR system. The measurement uncertainty is within ±2$K$ along the entire fiber but at the very end of it.

The flexibility of the system enables the use of a distributed fiber sensor in a wide variety of applications such as fire detection in tunnels and temperature measurements in connection with power cables or plant monitoring.

# REFERENCES

1. M. A. Farahani and T. Gogolla, "Spontaneous Raman Scattering in Optical Fibers with Modulated Probe Light for Distributed Temperature Raman Remote Sensing," *J. Lightwave Technology*, **17**, pp. 1379-1391, 1999.
2. U. Glombitza and E. Brinkmeyer, "Coherent Frequency Domain Reflectometry for Characterisation of Single-Mode Integrated-Optical Waveguides", *J. Lightwave Technology*, **11**, pp. 1377-1384, 1993.
3. Z. Zaixuan, L. Honglin, G. Ning, W. Jianfeng, W. Xiaobiao, Y. Xiangdong, F. Haiqi and I. S. Kim, "30km Distributed Optical Fiber Raman Photons Temperature Lidar," in *Lidar Remote sensing for Industry and Environment Monitoring III*, Proc. SPIE **4893**, pp. 78-82, 2003.
4. R. A. Serway, C. J. Moses, C. A. Moyer, *Modern Physics*, Sounders College, Orlando 1997.
5. G. Grau, W. Freude, *Optische Nachrichtentechnik*, 3rd Edition, Springer Verlag, 1991.
6. O. A. Wettingen, *Anwendung optischer und konventioneller Meßverfahren zur Beurteilung von Temperaturinhomogenitäten im Abgasstrahl eines Wellenleistungstriebwerks*, VDI Verlag, Düsseldorf, 2000.
7. Y. Tanabe, A. Takada, K. Ikawa and N. Bando, "An Improvement of the accuracy in the Distributed Fiber Temperature Measurement Using Raman Backscattering," *Optical Fiber Sensors*, **44**, pp. 537-543, 1989.
8. D. Garus, T. Gogolla, K. Krebber and F. Schliep, "Brillouin Optical Fiber Frequency Domain Analysis for Distributed Temperature and Strain Measurements," *J. Lightwave Technology*, **15**, pp. 654-662, 1997.
9. S. M. Maughan, H. H. Kee and T. P. Newson, "57-km single-ended spontaneous Brillouin-based distributed fiber temperature sensor using microwave coherent detection," *Optics Letters.*, **26**, pp. 331-333, 2001.
10. G. P. Agrawal, *Fiber-Optic Communication Systems*, John Wiley & Sons, New York, 1997.